

Combined reconstruction of weak and strong lensing data with WSLAP

J.M. Diego¹, M. Tegmark¹, P. Protopapas², H.B. Sandvik³.

¹ MIT Kavli Institute for Astrophysics and Space Research, Cambridge, MA 02139, USA.

² Harvard-Smithsonian Center for Astrophysics, 60 Garden Street, Cambridge, MA 02138, USA.

³ Max-Planck-Institut für Astrophysik, D-85748 Garching, Germany.

Draft version 28 July 2021

ABSTRACT

We describe a method to estimate the mass distribution of a gravitational lens and the position of the sources from combined strong and weak lensing data. The algorithm combines weak and strong lensing data in a unified way producing a solution which is valid in both the weak and strong lensing regimes. We study how the result depends on the relative weighting of the weak and strong lensing data and on choice of basis to represent the mass distribution. We find that combining weak and strong lensing information has two major advantages: it eliminates the need for priors and/or regularization schemes for the intrinsic size of the background galaxies (this assumption was needed in previous strong lensing algorithms) and it corrects for biases in the recovered mass in the outer regions where the strong lensing data is less sensitive. The code is implemented into a software package called WSLAP (Weak & Strong Lensing Analysis Package) which is publicly available at <http://darwin.cfa.harvard.edu/SLAP/>.

Key words: galaxies:clusters:general; methods:data analysis; dark matter

1 INTRODUCTION

Lensing problems usually distinguish between two regimes, strong and weak. In the strong lensing regime, a background source galaxy appears as multiple images, while in the weak lensing regime, its image suffers a small distortion which typically elongates it in a direction orthogonal to the gradient of the potential. The two problems are normally studied separately and, at best, they are combined afterward. Only a few attempts have been made to combine both regimes in the same analysis (e.g. Bradac et al. 2005, Broadhurst, Takada, Umetsu et al. 2005b).

The quality and quantity of strong and weak lensing data is growing rapidly, motivating the use of algorithms capable of making full use of the amount of information present in the images. In the early years of strong lensing data analysis, it was common to have only few constraints to work with. The small number of constraints made it impossible to extract useful information about the mass distribution of the lens without invoking a simple parametrization of the lens or the gravitational potential (Kneib et al. 1993, 1995, 1996, Broadhurst et al 1995, 2005a, Sand et al. 2002, Gavazzi et al. 2004). The common use of parametric models requires making educated guesses about the cluster mass distribution, for instance that the dark matter halos trace the luminosity of the cluster or that galaxy profiles possess

certain symmetries.

Nowadays, it is possible to obtain strong lensing images around the center of galaxy clusters with hundreds of arcs (Broadhurst et al. 2005a), where each arc contributes with several effective constraints in the process of solving for the projected mass distribution of the lens. In addition, weak lensing measurements provide shear constraints over a larger field of view. When added together, the number of constraints can be sufficiently high that non-parametric methods can be used in the reconstruction of the mass. With such a large number of constraints, non-parametric methods have a chance to compete with the parametric ones, complementing their results and raising interesting questions if significant disagreements are found between the two methodologies.

Non-parametric approaches have been previously explored in several papers (Saha et al. 1997, Abdelsalam et al. 1988b, 1998c, Trotter et al. 2000, Williams & Saha 2001, Warren & Dye 2003, Saha & Williams 2004, Bradac et al. 2005, Treu & Koopmas 2004) and more recently in Diego et al. (2005a) (hereafter **paper I**). In paper I, the authors showed that it is possible to non-parametrically reconstruct a generic mass profile (with substructure) provided that the number of strongly lensed arcs with known redshifts is sufficiently large. They developed a package called SLAP upon which WSLAP is based. Paper I also showed how work-

arXiv:astro-ph/0509103v1 5 Sep 2005

ing with extended images rather than just their positions adds enough constraints to solve the regularization problem found in other non-parametric algorithms (see Kochanek et al. 2004 for a discussion of this issue). An application of the method using SLAP on data from A1689 can be found in Diego et al. 2005b (hereafter **paper II**).

Most of the literature on lensing observations is based on either weak or strong lensing data. Only few papers have attempted to combine both weak and strong lensing data (e.g Bradac et al. 2005, Broadhurst, Takada, Umetsu et al. 2005b). The main advantage of combining both regimes is that they complement each other, filling the gaps and correcting the deficits of each other. Strong lensing data is particularly sensitive to the central mass distribution of the lens but is relatively insensitive to the outer regions. On the other hand, weak lensing cannot capture the fine details in the central regions but can trace the mass distribution further out than strong lensing data. One of the problems of modeling weak lensing data is the so-called mass-sheet degeneracy. Strong lensing can break this degeneracy if several arcs are observed and the sources of these arcs span a wide range of redshifts. Some algorithms have been proposed for combining the weak and strong lensing regimes (Abdelsalam et al. 1998a; Bridle et al. 1998; Saha, Williams and Abdelsalam 1999; Kneib et al. 2003; Smith et al. 2004; Bradac et al 2004), but usually they need to assume a prior on the mass (Kneib) or luminosity (Abdelsalam) or regularize the problem (Bradac, Abdelsalam). One of the purposes of this paper is to show how the above assumptions can be eliminated and that a well defined likelihood can be defined for the combined weak and strong lensing data set.

2 WSLAP AND STRONG LENSING

The fundamental problem in lens modeling is the following: Given the N_θ positions of lensed images, θ , what are the corresponding positions β of the background galaxies and the mass distribution $m(\theta)$ of the lens? Mathematically this entails inverting the lens equation

$$\beta = \theta - \alpha(\theta, m(\theta)) \quad (1)$$

where $\alpha(\theta)$ is the deflection angle created by the lens which depends on the observed positions, θ . Each observed position θ contributes with two constraints, $\theta = (\theta_x, \theta_y)$, so we have $2N_\theta$ strong lensing constraints.

The deflection angle α at the position θ , is found by integrating the contributions from the whole mass distribution:

$$\alpha(\theta) = \frac{4G}{c^2} \frac{D_{ls}}{D_s D_l} \int m(\theta') \frac{\theta - \theta'}{|\theta - \theta'|^2} d\theta' \quad (2)$$

where D_{ls} , D_l , and D_s are the angular distances from the lens to the source galaxy, the distance from the observer to the lens and the distance from the observer to the source galaxy respectively. In equation (2) we have made the usual thin lens approximation so the mass $m(\theta')$ is the projected mass along the line of sight θ' . From the deflection angle one can easily derive the magnification produced by the lens at a given position:

$$\mu^{-1}(\theta) = 1 - \frac{\partial \alpha_x}{\partial x} - \frac{\partial \alpha_y}{\partial y} + \frac{\partial \alpha_x}{\partial x} \frac{\partial \alpha_y}{\partial y} - \frac{\partial \alpha_x}{\partial y} \frac{\partial \alpha_y}{\partial x} \quad (3)$$

We find it convenient to expand the projected mass distribution in an set of basis functions:

$$m(x, y) = \sum_l c_l f_l(x, y), \quad (4)$$

where $f_l(x, y)$ are the basis functions and c_l the coefficients of the decomposition. Here $f_l(x, y)$, can be any sort of 2D function. For instance, one can choose orthogonal polynomials like the Legendre or Hermite polynomials. Or one can use Fourier or wavelet functions as the basis. We find that the best results are obtained using compact basis functions defined on a gridded version of the mass distribution like the ones used in papers I and II, since using extended ones tends to over-produce arcs in the final result — see however Sandvik et. al. (in preparation) for a novel approach to this problem. In papers I and II we used for f_l Gaussians with varying widths defined in a multi-resolution grid. In this paper we will focus on compact bases and will compare the results using three different compact bases.

After decomposing the mass as in equation (4), equation (2) can be rewritten as

$$\alpha(\theta_j) = \lambda_j \sum_l c_l \int f_l(\theta') \frac{\theta - \theta'}{|\theta - \theta'|^2} d\theta' = \lambda_j \sum_l c_l \tilde{f}_l(\theta_j), \quad (5)$$

where all the constants and distance factors are absorbed into the variable λ_j . Note that there is a different λ_j for each source since λ_j includes the distance factors D_l , D_s and D_{ls} which vary for each source. The factor $\tilde{f}_l(\theta_j)$ is the convolution of the basis function f_l with the kernel $(\theta - \theta')/|\theta - \theta'|^2$ evaluated at the point θ :

$$\tilde{f}_l(\theta_j) \equiv \int f_l(\theta') \frac{\theta - \theta'}{|\theta - \theta'|^2} d\theta'. \quad (6)$$

If now we define the matrix Υ by

$$\Upsilon_{jl} = \lambda_j \tilde{f}_l(\theta_j), \quad (7)$$

then all the constraints given by equation (1) can be expressed in the simple form

$$\Theta = \Upsilon \mathbf{c} - \beta. \quad (8)$$

where Θ is the array (vector) containing all the θ positions (θ_x and θ_y). The matrix Υ has a straightforward physical interpretation: the element Υ_{jl} is just the deflection angle created by the basis function f_l at sky position θ_j . Note that since θ_j has two components (the x and y components), there are two corresponding elements in Υ .

If we group all the unknowns in our problem (both β and \mathbf{c} or the mass in each cell) into a new vector \mathbf{x} , then equation (8) can be rewritten in the more compact form

$$\Theta = \Lambda \mathbf{x}, \quad (9)$$

where Λ is a $2N_\theta \times (N_c + 2N_s)$ -dimensional matrix and \mathbf{x} is the $(N_c + 2N_s)$ -dimensional vector containing all the unknowns in our problem (see paper I), *i.e.*, the N_c cell masses m_l (or coefficients c_l), and the $2N_s$ central positions β_o (x and y) of the N_s sources.

3 ADDING WEAK LENSING

So far we have focused on solving a system of linear equations corresponding to strong lensing data. If weak lensing

information is available, it can be easily incorporated into equation (9), allowing us to find the combined solution of the weak plus strong lensing as we will see below.

Given the gravitational potential ψ , the shear is defined in terms of the second partial derivatives of the potential ψ (the Hessian of ψ):

$$\psi_{ij} = \frac{\partial^2 \psi}{\partial \theta_i \partial \theta_j}, \quad (10)$$

$$\gamma_1(\theta) = \frac{1}{2}(\psi_{11} - \psi_{22}) = \gamma(\theta) \cos[2\varphi], \quad (11)$$

$$\gamma_2(\theta) = \psi_{12} = \psi_{21} = \gamma(\theta) \sin[2\varphi], \quad (12)$$

where $\gamma(\theta)$ is the amplitude of the shear and φ its orientation. The shear can be computed in a way very similar to the magnification μ yielding

$$\gamma_1 = \frac{1}{2} \left(\frac{\partial \alpha_x}{\partial x} - \frac{\partial \alpha_y}{\partial y} \right), \quad (13)$$

$$\gamma_2 = \frac{\partial \alpha_x}{\partial y} = \frac{\partial \alpha_y}{\partial x}. \quad (14)$$

The amplitude and orientation of the shear are given by

$$\gamma = \sqrt{\gamma_1^2 + \gamma_2^2}, \quad (15)$$

$$\varphi = \frac{1}{2} \text{atan}\left(\frac{\gamma_2}{\gamma_1}\right). \quad (16)$$

Given a number of shear measurements, an equation similar to (8) can be written for the shear:

$$\begin{pmatrix} \gamma_1 \\ \gamma_2 \end{pmatrix} = \begin{pmatrix} \mathbf{\Delta}_1 \\ \mathbf{\Delta}_2 \end{pmatrix} \mathbf{c}, \quad (17)$$

where each element in the matrices $\mathbf{\Delta}_1$ and $\mathbf{\Delta}_2$ represents the contribution to the shear (γ_1 and γ_2 respectively) of each one of the basis functions. The expression for Δ_{ij} can be easily derived from equations (7), (13) and (14). The explicit form of Δ_{ij} is given in Diego et al. (2005d).

After combining the strong and weak lensing regimes by regrouping the observed θ -positions of the strongly lensed galaxies and the measured shear, the new measurement vector $\mathbf{\Phi}$ will have the structure

$$\mathbf{\Phi}^t = (\theta_x, \theta_y, \gamma_1, \gamma_2), \quad (18)$$

and the corresponding system of linear equations representing the lens equation reads

$$\begin{pmatrix} \theta_x \\ \theta_y \\ \gamma_1 \\ \gamma_2 \end{pmatrix} = \begin{pmatrix} \mathbf{\Upsilon}_x & \mathbf{I}_x & \mathbf{0} \\ \mathbf{\Upsilon}_y & \mathbf{0} & \mathbf{I}_y \\ \mathbf{\Delta}_1 & \mathbf{0} & \mathbf{0} \\ \mathbf{\Delta}_2 & \mathbf{0} & \mathbf{0} \end{pmatrix} \begin{pmatrix} \mathbf{c} \\ \beta_x \\ \beta_y \end{pmatrix}, \quad (19)$$

where we have explicitly expanded the matrix \mathbf{A} and the vector of unknowns \mathbf{x} into their components. In the above equation, the matrix $\mathbf{0}$ contains all zeros while the ij elements in matrix \mathbf{I}_x are ones if the θ_i pixel (x -coordinate) is coming from the β_j source (y -coordinate) and zero otherwise. The matrix \mathbf{I}_y is defined in an analogous way for the y -coordinates. The above equation written in compact form is simply

$$\mathbf{\Phi} = \mathbf{\Gamma} \mathbf{x}. \quad (20)$$

In summary, we have formulated the full weak and strong

lensing problem in a manner where the observables $\mathbf{\Phi}$ depend linearly on the unknowns \mathbf{x} , so all the complicated physics and geometry is conveniently encoded into the known matrix $\mathbf{\Gamma}$.

In principle, an exact solution for \mathbf{x} exists if the inverse of $\mathbf{\Gamma}$ exists (i.e $\mathbf{x} = \mathbf{\Gamma}^{-1} \mathbf{\Phi}$). However, in most cases, $\mathbf{\Gamma}$ is singular and therefore does not have an inverse (some of the eigenvalues are basically zero within rounding errors), so a direct inversion of the problem is not possible. Furthermore, even when the inverse of $\mathbf{\Gamma}$ exists, we may not be interested in finding the exact solution, but rather in an approximate solution of equation (20). The reason is twofold. The definition of \mathbf{x} assumed that the source galaxies responsible for the strong lensing arcs are point-like (that is, each source is defined only by its coordinates, β_x and β_y). This assumption is inaccurate as the galaxies will have some spatial extent, so we want the solution to allow for some residual in equation (20). Second, for the mass we have assumed that it is a superposition of certain basis functions, say cells. This assumption, although a good approximation, is also partially inaccurate, so we want to incorporate this in our analysis by allowing some residual ($|\mathbf{r}| > 0$) in the lens equation. This residual is defined as

$$\mathbf{r} \equiv \mathbf{\Phi} - \mathbf{\Gamma} \mathbf{x}. \quad (21)$$

4 SOLVING THE LENS PROBLEM

The fundamental task we are faced with is to obtain the coefficients \mathbf{c} , describing the lens surface mass density, and the positions β of the background galaxies in order for their combination to explain the observed arcs θ and the shear γ . In the previous section, we have shown how the unknowns of the problem can be combined into a vector \mathbf{x} , the observed data into another vector, $\mathbf{\Phi}$, and the connection between the two is given by the matrix $\mathbf{\Gamma}$. These three elements relate to each other through the system of linear equations (20).

We adopt a Bayesian approach to solving the problem, finding the solution \mathbf{x} that maximizes the likelihood function.

$$\mathcal{L}(\mathbf{x}) = e^{-\frac{1}{2} \chi^2}, \quad (22)$$

where we have assumed that the residual \mathbf{r} is Gaussian distributed. The χ^2 is defined as

$$\chi^2 = \mathbf{r}^t \mathbf{C}^{-1} \mathbf{r}, \quad (23)$$

where \mathbf{C} is the covariance matrix of the residual \mathbf{r} . We model the residuals as uncorrelated (\mathbf{C} is diagonal) and that the elements on the diagonal are equal to either σ_θ^2 or σ_γ^2 , where the former is associated with the expected residual variance in the strong lensing data and the latter is for the expected residual variance in the shear measurements.

We will extensively discuss how to best choose \mathbf{C} below in Section 6.2. For the main calculations in this paper, we assume that the rms error σ_θ is of the order of a few pixels in the source plane, and model σ_γ as uniform over the field of view, equal to 0.005 for both the γ_1 and γ_2 components. Errors in shear measurements can be in the range of a few percent for well calibrated experiments (e.g Hirata et al. 2005, Heymans et al. 2005). A value of $\sigma_\gamma = 0.005$ is at the percent level for a typical cluster. The covariance matrix \mathbf{C}

can also incorporate a measure of the noise in the data both in the strong and weak lensing.

We will now explore two alternative approaches for finding the solution that maximizes the likelihood (minimizes the χ^2).

4.1 Bi-conjugate Gradient Method

Substituting equation (21) into equation (23),

$$\begin{aligned}\chi^2 &= (\boldsymbol{\Phi} - \boldsymbol{\Gamma}\mathbf{x})^t \mathbf{C}^{-1} (\boldsymbol{\Phi} - \boldsymbol{\Gamma}\mathbf{x}) \\ &= \boldsymbol{\Phi}^t \mathbf{C}^{-1} \boldsymbol{\Phi} - 2\boldsymbol{\Phi}^t \mathbf{C}^{-1} \boldsymbol{\Gamma}\mathbf{x} + \mathbf{x}^t \boldsymbol{\Gamma}^t \mathbf{C}^{-1} \boldsymbol{\Gamma}\mathbf{x} \\ &= b - \mathbf{a}^t \mathbf{x} + \frac{1}{2} \mathbf{x}^t \mathbf{A} \mathbf{x},\end{aligned}\quad (24)$$

where we have defined the constant $b \equiv \boldsymbol{\Phi}^t \mathbf{C}^{-1} \boldsymbol{\Phi}$, the vector $\mathbf{a} \equiv 2\boldsymbol{\Gamma}^t \mathbf{C}^{-1} \boldsymbol{\Phi}$ and the matrix $\mathbf{A} \equiv 2\boldsymbol{\Gamma}^t \mathbf{C}^{-1} \boldsymbol{\Gamma}$.

Minimizing this by setting the derivative with respect to \mathbf{x} equal to zero gives a formal solution $\mathbf{x} = \mathbf{A}^{-1} \mathbf{a}$. This is not useful in practice, however, since $\boldsymbol{\Gamma}$ (and therefore also \mathbf{A}) is normally rather singular. In paper I, we found a simple regularization technique that gives physically reasonable results: minimizing χ^2 using the iterative bi-conjugate gradient method (Press et al. 1997), but stopping once an approximate solution of equation (20) had been found rather than continuing to iterate toward the formal solution. Specifically, the bi-conjugate gradient method performs successive minimizations which are carried out in a series of orthogonal conjugate directions with respect to the metric \mathbf{A} . The algorithm starts with an initial guess for the solution (for instance $\mathbf{x}_0 = \mathbf{0}$). Then the algorithm chooses as a first minimization direction the gradient $\nabla \chi^2$ at \mathbf{x}_0 . Then it minimizes in directions which are conjugate to the previous ones until it reaches the minimum or the χ^2 is smaller than certain target value ϵ . We will discuss later how to choose ϵ — we will find that combining weak and strong lensing makes the choice of ϵ much less relevant than when only strong lensing data is used in the analysis.

4.2 Nonnegative quadratic programming

Although the bi-conjugate gradient method is a fast and effective way to find an approximate solution, it is not ideal. The regularization procedure was required because certain modes in the mass distribution corresponded to eigenvalues near zero in the matrix \mathbf{A} . Plotting these unconstrained modes shows that they all oscillate, trading off positive mass in some places against unphysical negative mass elsewhere. Without regularization, the solution can include such modes of significant amplitude, involving negative mass in certain cells. Both the regularization problem and negative mass problem can therefore be eliminated in one fell swoop by using a constrained minimization algorithms that only minimizes χ^2 in the physically meaningful region of the parameter space \mathbf{c} where all masses are non-negative. Our case is particularly simple: we are minimizing a quadratic function of \mathbf{x} subject to constraints on \mathbf{x} that are linear. This is a well studied problem in optimization theory, and several methods have been proposed in the context of quadratic programming (QADP). In this paper we will explore the approach of Sha, Saul & Lee (2002) known as multiplicative updates for nonnegative quadratic programming.

Following Sha et al. (2002), we can minimize the quadratic objective function

$$f(\mathbf{x}) = \frac{1}{2} \mathbf{x}^t \mathbf{A} \mathbf{x} + \mathbf{a}^t \mathbf{x} \quad (25)$$

subject to a non-negative mass constraint, *i.e.*, the constraint that $m_i \geq 0$ for all i , where m_i is the mass at position i . Note that when compared with equation (24), we have changed the sign of vector \mathbf{a} to keep the same notation of Sha et al. (2002). In our vector \mathbf{x} , the mass distribution is represented by expansion coefficients \mathbf{c} rather than cell masses \mathbf{m} , and equation (4) shows that these two vectors are related by

$$\mathbf{m} = \mathbf{F} \mathbf{c}, \quad (26)$$

where the element \mathbf{F}_{il} is the value of the basis function f_l at position i . We can therefore make the substitution $\mathbf{x} = \mathbf{F}^{-1} \mathbf{m}$ in equation (25) and rewrite it as a function of a transformed vector denoted \mathbf{x}' which equals \mathbf{x} except that the elements defining the mass distribution are $\mathbf{m} = \mathbf{F} \mathbf{c}$ rather than \mathbf{c} :

$$f'(\mathbf{x}') = \frac{1}{2} \mathbf{x}'^t \mathbf{A}' \mathbf{x}' + \mathbf{a}'^t \mathbf{x}', \quad (27)$$

where \mathbf{a}' is the same as \mathbf{a} but with the elements related to masses multiplied by \mathbf{F}^{-1} , and \mathbf{A}' is the same as \mathbf{A} but with the sub-matrix related to masses multiplied by \mathbf{F}^{-1} both from the left and from the right. In general, the dimensionality of \mathbf{x}' can be different than the dimensionality of \mathbf{x} . However, to keep the problem simple, we assume that the masses in equation (26) are evaluated only at the central position of each cell. That makes the dimensions of \mathbf{x} and \mathbf{x}' equal and m_i can be interpreted as simply the total projected mass in the i^{th} -cell. Since the positions β can be also made positive (by defining the origin of the coordinates in the left bottom corner of the field of view), all components in the vector \mathbf{x}' (m_i and β_j) have to be positive.

In conclusion, we wish to minimize equation (27) subject to the constraints that all elements $x'_i \geq 0$. We solve this problem iteratively using the multiplicative update technique of Sha, Saul & Lee (2002). For simplicity of notation, we suppress all primes from equation (27) below. Let us split the matrix \mathbf{A} into its positive and negative parts \mathbf{A}^+ and \mathbf{A}^- such that $\mathbf{A} = \mathbf{A}^+ - \mathbf{A}^-$, where $A_{ij}^+ \equiv A_{ij}$ if $A_{ij} > 0$ and 0 otherwise and $A_{ij}^- \equiv -A_{ij}$ if $A_{ij} < 0$ and 0 otherwise. The solution is iteratively updated by the rule

$$x_{i+1} = x_i \delta_i, \quad (28)$$

where the multiplicative updates δ_i are defined by

$$\delta_i = \frac{-a_i + \sqrt{a_i^2 + 4(\mathbf{A}^+ \mathbf{x})_i (\mathbf{A}^- \mathbf{x})_i}}{2(\mathbf{A}^+ \mathbf{x})_i}. \quad (29)$$

It is easy to see that generic quadratic programming problems have a single unique minimum. Let \mathbf{x}^* denote this global minimum of $f(\mathbf{x})$ (within the non-negative mass part of parameter space). Let us prove that convergence of the iteration equation (29) corresponds to this minimum \mathbf{x}^* . At this point, one of two conditions must apply for each component x_i^* : Either (i) $x_i^* > 0$ and $\frac{\partial f}{\partial x_i}(\mathbf{x}^*) = 0$ or (ii) $x_i^* = 0$ and $\frac{\partial f}{\partial x_i}(\mathbf{x}^*) \geq 0$. Now since

$$\frac{\partial f}{\partial x_i}(\mathbf{x}^*) = (\mathbf{A}^+ \mathbf{x})_i - (\mathbf{A}^- \mathbf{x})_i + a_i, \quad (30)$$

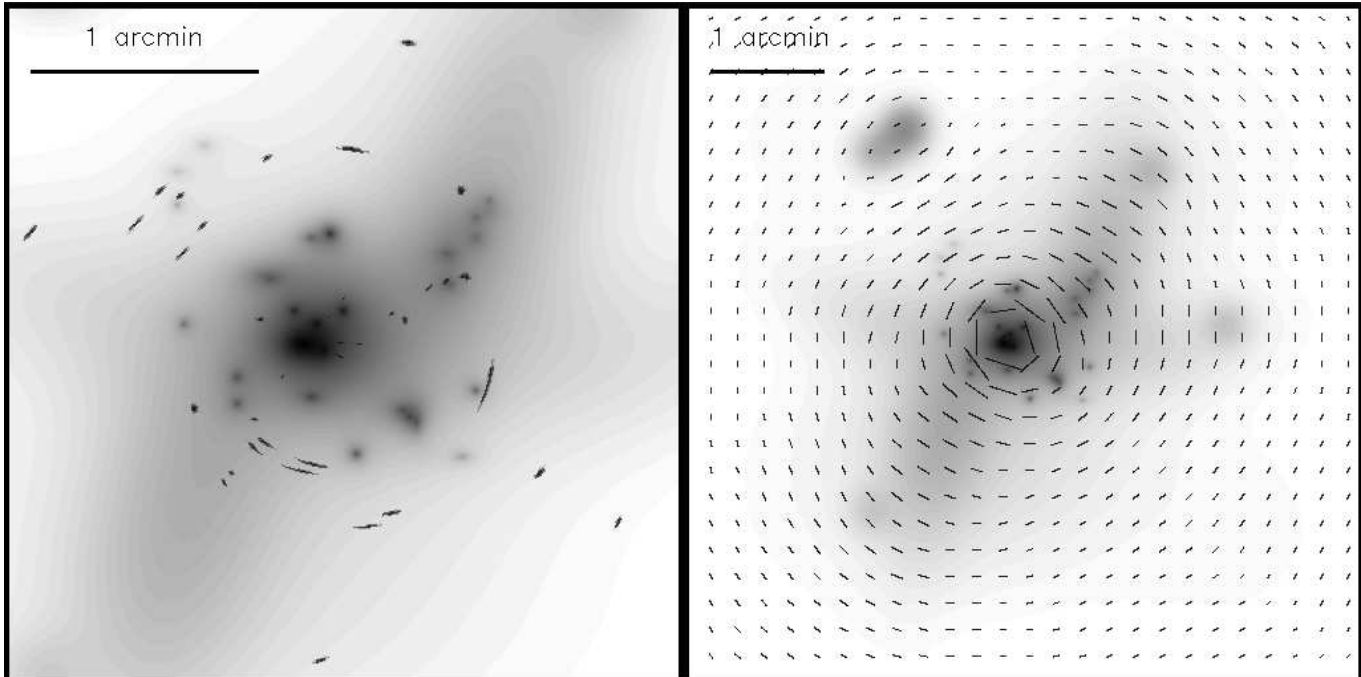


Figure 1. Original mass used to test the algorithm (at $z=0.4$). The mass is built out of a superposition of 30 NFW profiles with added ellipticities. The total mass in the field of view (6 arcmin) is $1.17397 \times 10^{15} h^{-1} M_{\odot}$. The left panel shows the central region (3 arcmin, $0.663 \times 10^{15} h^{-1} M_{\odot}$) and the strongly lensed galaxies. These arcs are lensed images of 9 galaxies between redshifts 1 and 6.5. The right panel (6 arcmin) shows the shear field and the outer regions of the cluster.

the multiplicative updates in both cases (i) and (ii) take the value $\delta_i = 1$, the minimum is a fixed point. Conversely, a fixed point of the iteration must be the minimum \mathbf{x}^* .

5 SIMULATIONS

Testing the algorithm with simulations is essential, not only to prove its feasibility but also to identify its failures and weaknesses. In this paper, we will show some results using a simulated cluster with a particularly rich structure. The motivation for this is twofold. First, using a highly asymmetric distribution motivates the use of non-parametric methods where no assumptions about the distribution of the mass are needed. Second, asymmetries may play a role introducing biases in the result which we may want to study.

Also, with simulations we can test how different choices for f_i and \mathbf{C} affect the result. This last step is important since f_i and \mathbf{C} are basically the only assumptions made in the process of fitting the data.

The simulated data are made of a combination of 3 basic ingredients:

- 1) the lens mass distribution that we will try to recover,
- 2) the arcs observed in the central region of our field of view that will constitute the strong lensing part of the data,
- 3) the shear measured over the entire field of view which will constitute the weak lensing part of the data.

5.1 Mass distribution

In order to test the algorithm, we will use a simulated cluster with abundant internal structure. The cluster is placed at redshift $z=0.4$. It has a highly elliptical extended large scale component at large scale and the central region has several clumps surrounding the central peak. These clumps are generated from NFW profiles with added ellipticities. There is also a filamentary component crossing the field of view. The simulated cluster has a total projected mass of $1.174 \times 10^{15} h^{-1} M_{\odot}$ over the field of view (6 arcmin) and is shown in figure 1. This field of view corresponds to a scale of $1.35 h^{-1}$ Mpc and normally covers more than half the virial radius expected for clusters with this mass.

5.2 Strong lensing data

To generate the arcs, we place several sources behind the cluster. The sources have redshifts between $z = 1.0$ and $z = 6.5$. We consider 9 sources in this redshift range. The arcs produced by the combination lens-sources are shown in figure 1 (left panel). These arcs will constitute the strong lensing part of our data set. We use all the pixels containing part of one arc in the previous image. There are 621 of these pixels. All the sources have at least two lensed images in the previous plot. Some sources appear as many as five times. Although we search for multiple images only in the central part of the field of view (3×3 arcmin²), we use the mass over the entire field of view (6×6 arcmin²) to calculate the deflection angle.

5.3 Weak lensing data

For the weak lensing part, we calculate the shear field over the entire 6×6 arcmin² field of view (or equivalently 1.35×1.35 (h⁻¹ Mpc)²). The shear is simulated assuming the sources have a medium redshift of $z = 3$. We consider that the observation is deep enough and that a shear measurement can be obtained after averaging areas of 14.5×14.5 arcsec² which renders 625 shear measurements over the field of view ($625 \gamma_1$ and $625 \gamma_2$). The shear field is shown in the right panel of figure 1.

Summarizing, the strong lensing data consist of $N_\theta = 621$ pixels distributed in about 40 strongly lensed images (or arcs) coming from 9 sources. Each pixel contributes as two data points (θ_x and θ_y). The shear is computed on a $N_\gamma = 25 \times 25$ grid over a field of view expanding 6 arcmin. Each shear measurement contributes also with two data points (γ_I and γ_{II}). The data vector, Φ is then an N -dimensional vector with $N = 2N_\theta + 2N_\gamma = 2 \times 612 + 2 \times 625 = 2492$. The number of unknowns N_x is the number of cells (or basis) N_c plus two times the number of sources N_s (the factor 2 coming from the x and y component), $N_x = N_c + 2N_s = 2 \times 500 + 2 \times 9 = 1018$ where we have assumed that the lens plane has been divided in 500 cells. The matrix \mathbf{A} ($= \mathbf{\Gamma}^t \mathbf{C}^{-1} \mathbf{\Gamma}$) is a $N_x \times N_x$ matrix, and the vectors \mathbf{x} and $\mathbf{a} = \mathbf{\Gamma}^t \mathbf{C}^{-1} \Phi$ have dimension N_x (\mathbf{A} and \mathbf{a} are defined below equation 24).

6 RESULTS

As in papers I and II, we start the minimization process assuming we know nothing about the mass distribution and use a regular grid to divide the lens plane. Also, as explained in paper I, a regular grid has the inconvenience that the small details of the mass distribution can not be described with enough accuracy. That means, the lens is less adaptable and will have problems reproducing the data. To avoid getting a very biased solution, the minimization process has to be stopped earlier than in the case where the grid reproduces finer details (bigger ϵ). Otherwise we will end up with an unphysical solution which tries to fit the data superposing big “chunks” of dark matter in the lens plane. Figure 2 shows the result after the first iteration. It also shows the grid used to decompose the plane of the surface mass into cells ($N_c = 256$ cells). The first iteration finds an elliptical distribution of mass in the right location but is unable to unveil any of the finer details of the mass distribution. The total mass in this first iteration is smaller than the original mass by 20%. Once we have a guess for the mass distribution, the adaptive grid can be constructed by splitting the cells with higher densities into smaller cells. Cells are split in an iterative process which subdivides the cells having higher densities into four smaller sub-cells. The splitting procedure stops when the goal number of cells is achieved, say $N_c = 500$. Each time a new grid is built, the $\mathbf{\Gamma}$ matrix has to be recomputed again. Each minimization step (new grid + new $\mathbf{\Gamma}$ + new solution) usually takes about 10 seconds on a 1 GHz processor. In figure 3 we show the result after 10 minimizations. The number of cells used in this case was $N_c = 500$. Note how the recovered mass reproduces well most of the original structure up to the limits of the field of view (compare with figure 1).

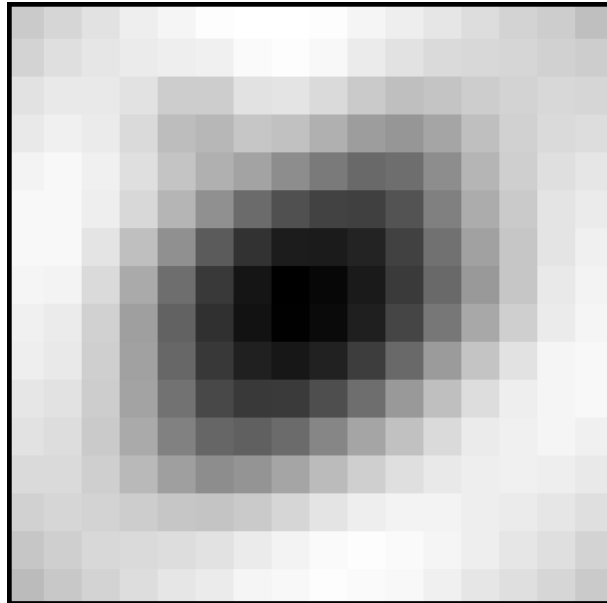


Figure 2. Recovered mass (6 arcmin) after first minimization (regular grid). The total mass is 20% smaller than the true one.

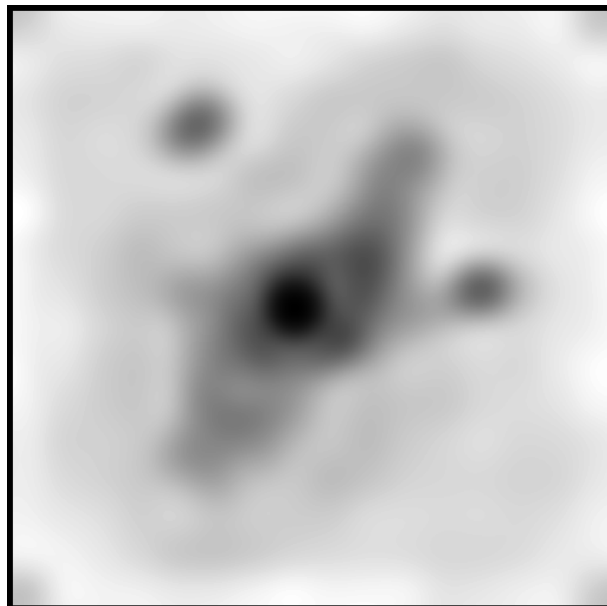


Figure 3. Recovered mass (6 arcmin) after 10 minimizations (multi-resolution grid). The total mass is 2% smaller than the true one. This result was obtained using the bi-conjugate gradient algorithm (1-2 seconds). The minimization is stopped when $\chi^2 \sim 10^{-11}$. Using quadratic programming, the result is very similar (see figure 4) but it takes several hours to converge.

Minimizing χ^2 using the nonnegative quadratic programming algorithm described above renders very similar results but the process can take up to several hours to converge. The main advantage of using QADP is that the solution converges to a mass distribution which is less biased with respect to the true mass than the *point source solution* given by the bi-conjugate gradient algorithm. In figure 4 we show the results obtained with QADP in the different scenarios, using SL data alone, using WL data alone

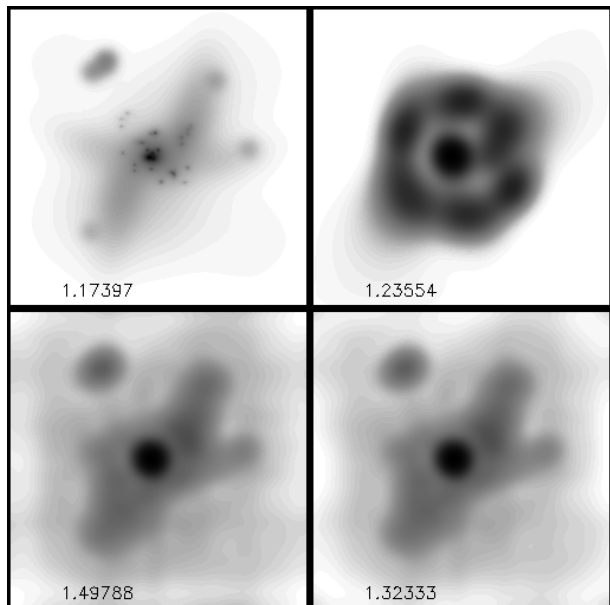


Figure 4. Results obtained with the QADP algorithm and using a regular grid of 32×32 cells. The field of view is 6 arcmin in all cases. From top to bottom and left to right, original mass, reconstructed mass with SL data only, reconstructed mass with WL only, and reconstructed mass with combined WL and SL data. The numbers at the bottom of each panel is the total mass in the field of view. QADP was left running until convergence (relative change in the total mass of 10^{-9}).

and combining both. The combination gives a better reconstructed mass than the other two. Note also, how using WL data alone over-predicts the total mass by almost 30% while the combination overpredicts the mass by only 12%. QADP does not suffer of the regularization problems of bi-conjugate gradient. There is no point source solution and the algorithm can be left running until convergence is achieved. The results presented above, correspond to the solution at the convergence point (relative change in the total mass less than 10^{-9}).

By comparing these results with the ones in papers I and II we see an improvement in the recovered mass profile. First, adding weak lensing allows the reconstruction to extend much further than the case where only strong lensing data is used. Second, in papers I and II we showed how the results may depend on the specific choice of ϵ . In particular, we showed that setting a very small ϵ produces a solution where the recovered sources are too small. This solution was called the *point source solution* in the previous papers I and II. Adding weak lensing partially solves this problem (see figure 5). The dependency with ϵ is much weaker when weak and strong lensing are combined together. When only strong lensing is used in the minimization (see papers I and II), the bi-conjugate gradient naturally tends to increase the mass in the center of the lens so the sources get more *compressed* in the center of the image (smaller χ^2). Adding weak lensing avoids the mass to grow too much in the center since that would not reproduce properly the observed shear field. On the other hand, using weak lensing alone has the potential problem of the mass-sheet degeneracy. Adding strong lensing acts as a regularizing component since a very specific amount of mass is needed in the central region to *focus* the

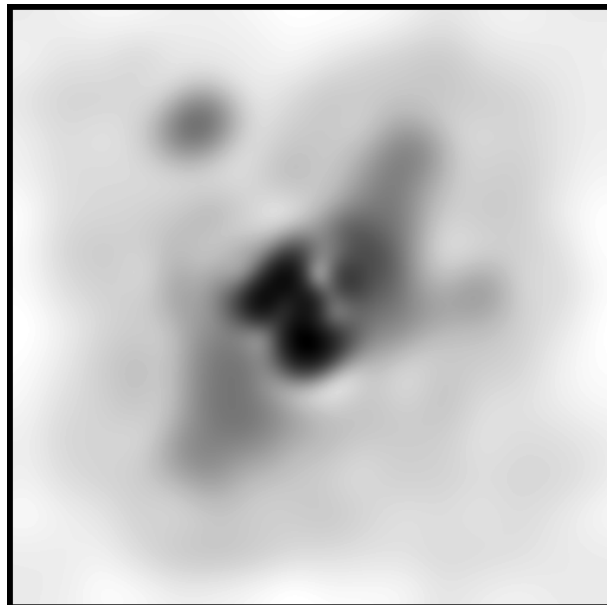


Figure 5. Point source solution in the 6 arcmin field of view obtained with the biconjugate gradient algorithm (absolute minimum of $\chi^2 \approx 10^{-13}$). The total mass is only 10% larger than the true one.

big arcs into compact sources at different redshifts.

Another important difference with papers I and II is that they used no covariance matrix (or more specifically, they assumed that $\mathbf{C} = \mathbf{I}$). The main reason to introduce a covariance matrix in the present paper is to properly weight the strong and weak lensing data. The covariance matrix can be also viewed as a way to allow for the instrumental noise and systematic error to play a role in the strong and weak lensing data, making one data set more relevant than the other if their measurements are more accurate.

6.1 Dependence on the covariance matrix, \mathbf{C}

The covariance matrix \mathbf{C} controls which information is more relevant in the χ^2 . The main advantage of a combined weak+strong lensing analysis is that we can get both the gradient of the mass distribution up to large radii from the weak lensing part and the overall mass normalization plus detailed internal distribution from the strong lensing part. The two regimes are properly weighted through the covariance matrix, \mathbf{C} . Giving more importance to the strong lensing data will produce a better estimate in the central regions but will produce a result relatively insensitive to the outer regions. On the other hand, increasing the relevance of the weak lensing will constrain better the outer regions but at the expense of losing accuracy in the normalization. A good example of this is shown in figure 6. In this example we vary the amplitude of the covariance of the shear map by two orders of magnitude. Making the shear covariance smaller increases the relative importance of the weak lensing in the minimization. On the other hand, increasing the shear covariance, reduces the overall importance of the weak lensing part. We found that values of the strong lensing and shear covariance around $\sigma_\theta = 10^{-5}$ rads (~ 2 arcsec)

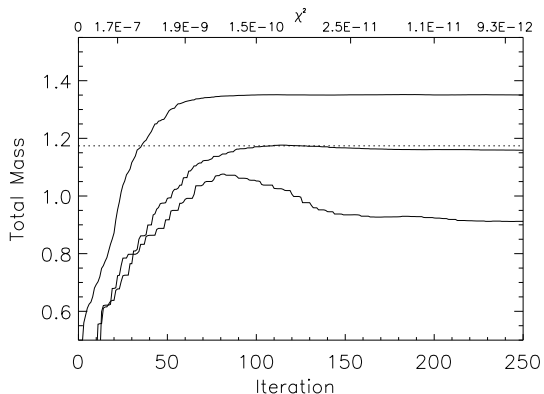


Figure 6. Total mass as a function of iteration number inside the bi-conjugate gradient routine. The true mass is shown as a flat dotted line. The three solid lines correspond to 3 assumptions on the covariance matrix \mathbf{C} . Middle curve, $\sigma_\theta = 3$ pixels and $\sigma_\gamma = 0.005$. Upper curve, σ_γ is 10 times smaller (WL dominates). Lower curve, σ_γ is 10 times larger (SL dominates). The upper x-axis shows the corresponding value of the χ^2 at each iteration.

and $\sigma_\gamma = 0.005$ produce an unbiased estimate of the total mass (see figure 6). The ratio of these two values is equal to $\sigma_\gamma = 0.005/\sigma_\theta = 500$. This ratio makes the contribution of the weak and strong lensing more or less equal in the χ^2 (see figure 7). We call this the *equal variance approach* since the dispersion of the $\mathbf{C}^{-1}\mathbf{\Upsilon}$ and $\mathbf{C}^{-1}\mathbf{\Delta}$ is more or less the same (see figure 7). Also in figure 6 we show the evolution of χ^2 with the iteration number. The χ^2 decreases quickly in the first iterations and reaches a *plateau* afterward. The bottom of the plateau is at $\chi^2 \approx 10^{-13}$. This solution corresponds to the *point source solution* identified in papers I and II (see figure 5). In opposition to what happened in the previous papers I and II, the point source solution does not deviate much from the real mass distribution. This is an important improvement since it shows how the combination of weak and strong lensing stabilizes the solution and waives the need of any prior on the size of the sources (this prior was needed in papers I and II).

The recovered 1-dimensional profiles show clearly the effect of changing the relative weights of the shear and strong lensing data. In figure 8 we show the same cases as in figure 6. The upper thin solid line corresponds to the case where the weak lensing is given more relative weight while the lower thin solid line is the opposite case where the strong lensing is given more importance. The two middle profiles (dotted and dashed line) correspond to the intermediate case where the histograms of $\mathbf{\Upsilon}$ and $\mathbf{\Delta}$ (re-scaled by \mathbf{C}^{-1}) share more or less the same scale (figure 7).

6.2 Alternative choices for \mathbf{C}

So far we have considered only the case where σ_θ and σ_γ are constants. The *equal variance approach* consists on choosing σ_γ such that the dispersion of the $\mathbf{C}^{-1}\mathbf{\Upsilon}$ and $\mathbf{C}^{-1}\mathbf{\Delta}$ matrices are more or less the same. In other words, this choice for \mathbf{C}^{-1} makes the contribution from the weak and strong lensing more or less equal (when $N_\theta \approx N_\gamma$). This choice produces satisfactory results as we have seen above.

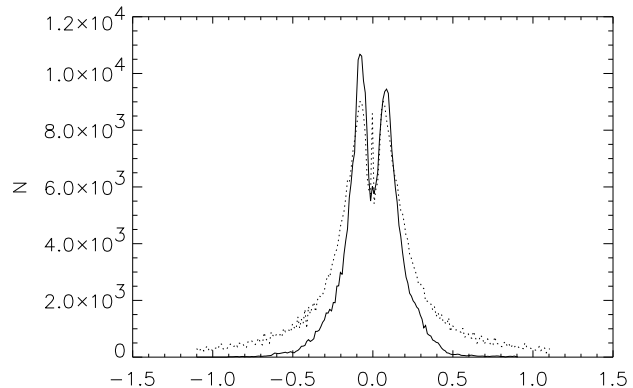


Figure 7. Histograms of the elements of $\mathbf{\Upsilon}_y$ (solid) and $\mathbf{\Delta}_2$ matrices. $\mathbf{\Upsilon}_y$ has been multiplied by a factor 500. This factor is roughly the ratio between σ_θ (3 pixels or 2.1 arcsec = 10^{-5} rad) and σ_γ (0.005) in the covariance matrix \mathbf{C} . These values for σ_θ and σ_γ make the $\mathbf{C}^{-1}\mathbf{\Upsilon}$ and $\mathbf{C}^{-1}\mathbf{\Delta}$ to have more or less the same variance. We refer to this case as the *equal variance approach*. The histogram of $\mathbf{\Upsilon}_y$ extends up to ± 40 . Large values in $\mathbf{\Upsilon}$ occur when the shear is measured near the caustics.

Since \mathbf{C} can be seen as the matrix containing the covariances of the data points, one may feel tempted to play with different weights for the data set. For instance, one may consider giving more relative importance to the smaller radial arcs than to the bigger tangential arcs. This is motivated by the fact that the residual of the strong lensing part is more clearly dominated by the big tangential arcs than by the small radial ones. We have tried different weighting factors in the matrix \mathbf{C} and found that the best results are obtained when the weight of the strong lensing data, σ_θ , is homogeneous over the field of view, that is, all data points are given the same importance independently of whether they are forming part of a giant arc or a tiny radial arc. Weighting the radial arcs more than the tangential ones produces biased results in the recovered mass distribution, including the position of the central peak. A good result is obtained also when the weight is proportional to the fraction of pixels in the system compared with the total number of pixels in all systems. In this case, the results are very similar to the ones obtained with an homogeneous weight in \mathbf{C} .

6.3 Dependence on the basis f_i

In this section, we will discuss the role of the basis functions f_i used to decompose the mass (equation 4).

We found that in general compact basis give better results than extended ones. As an example, in figure 9 we show the reconstructed profiles using three different sets of basis functions:

- i) A Gaussian basis centered in each cell with a width, σ , equal to two times the size of the cell,

$$G(r) \propto \exp(-r^2/2\sigma^2). \quad (31)$$

- ii) An isothermal sphere with a core of the same scale σ ,

$$I(r) \propto \frac{1}{r + \sigma}. \quad (32)$$

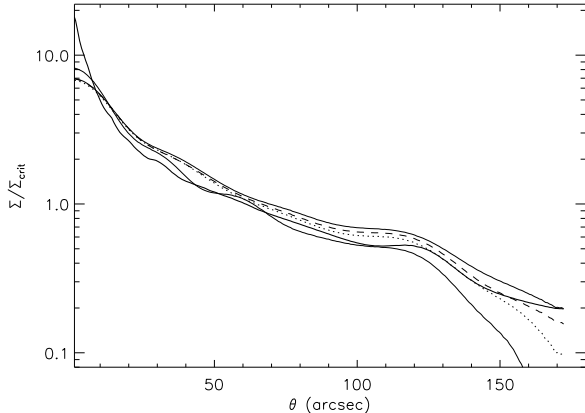


Figure 8. Original profile (thick solid line) vs reconstructed ones. Dotted line is the recovered profile using the fast bi-conjugate gradient algorithm while dashed line is the result obtained with QADP. The top thin solid line corresponds to the upper curves of figure 6 (WL dominated case). The bottom thin solid line correspond to the lower curve of figure 6 (SL dominated case). Note how the strong lensing dominated analysis reproduces better the central peak but fails in the tails and how the situation reverses when we increase the relative importance of the weak lensing in the covariance matrix \mathbf{C} .

iii) A power law also with a core of the same scale σ ,

$$P(r) \propto \frac{1}{r^2 + \sigma}. \quad (33)$$

The results obtained with the isothermal sphere and the power law show a constant sheet excess in the surface mass density which is probably due to the extended tails of the basis. These two basis reproduce well the central parts but fail in predicting the right density in the outer regions. This behavior may be a manifestation of the mass-sheet degeneracy.

7 CONCLUSIONS

In this paper, we have presented a way of consistently combining strong and weak lensing using a non-parametric method (WSLAP) which does not rely on any prior on the luminosity and does not suffer from significant regularization problems. Finding the solution through the bi-conjugate gradient still is affected by minor regularization problems as the minimization has to be stopped before the absolute minimum is reached. This is needed to avoid the *point source solution*. However, we have seen how even the point source solution can be a good estimation of the mass when weak and strong lensing are combined. In previous papers using only strong lensing, we found that the point source solution obtained with the bi-conjugate gradient was a bad estimate of the mass. On the other hand, the solution obtained with QADP does not suffer of regularization problems. Imposing the constraint that the masses have to be positive is a natural way to regularize the solution.

Adding weak lensing has two major effects on the solution; i) when minimizing the quadratic function with standard algorithms (for instance the bi-conjugate gradient) the

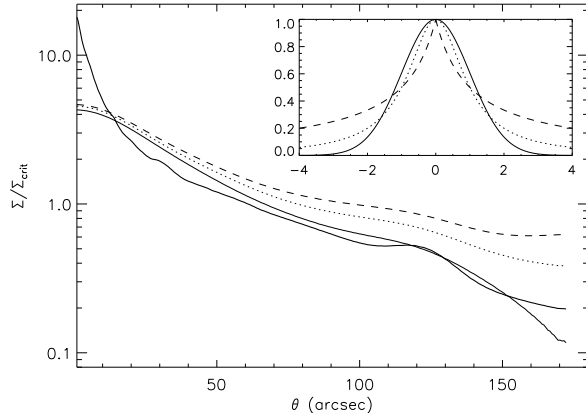


Figure 9. Original profile (thick solid line) vs reconstructed ones. From top to bottom. Using as basis f_i isothermal spheres (dashed), power laws (r^{-2}) (dotted) and Gaussians (thin solid line). The inner plot shows the three basis for the same scale $\sigma = 1$. Gaussian (solid), power law ($r^2 + \sigma$)⁻¹ (dotted) and isothermal ($r + \sigma$)⁻¹ (dashed). Basis with extended tails act adding a constant surface mass density to the overall mass. Compact functions like the Gaussian can concentrate the mass closer to the cell where they are positioned.

result is basically insensitive to the threshold ϵ where the minimization is stopped since the negative masses which appear when ϵ is too small can not reproduce the shear field properly, ii) the profile can be better reproduced inside and beyond the position of the big arcs. The weak lensing data allow us to eliminate the use of any *prior* on the physical size of the sources and to better constrain the range of solutions, thus adding more robustness to the final result.

The method allows the freedom to make two choices, for the covariance matrix \mathbf{C} and the basis functions f_i , and we quantified the impact of both on systematic errors in the mass reconstruction. We found that the *equal variance approach* for the covariance matrix renders satisfactory results. Giving more relative importance to the radial than to the tangential arcs produces a biased solution for the mass. Weighting the arc systems proportional to their area in the sky produces similar results as in the case of the equal variance approach. Regarding the basis functions, we found that functions f_i which are compact produce better results than extended functions, specially in describing the weak lensing part of the data. This fact may be a manifestation of the mass-sheet degeneracy in the weak lensing data.

This paper is more of an illustration of how to extend the methodology of SLAP (papers I and II) to include weak lensing than a detailed description of the capabilities and failures of the WSLAP approach. However, although an illustration, this paper demonstrates the usefulness of non-parametric methods when combining weak and strong lensing.

Much work needs still to be done to address possible systematic issues, but as described in paper II, most of this work will have to be done when WSLAP is applied to real data. The systematics may depend on the specific nature of the problem (number of sources, geometry and redshift of

the lens, quality of the data). Future improvements will include adding photometric information and a better modeling of the sources (Sandvik et al. in preparation).

WSLAP is now available to the community at:

<http://darwin.cfa.harvard.edu/SLAP/>.

8 ACKNOWLEDGMENTS

This work was supported by NSF CAREER grant AST-0134999, NASA grant NAG5-11099, the David and Lucile Packard Foundation and the Cottrell Foundation. The authors would like to thank David Hogg for useful discussions on quadratic programming and Elizabeth E. Brait for useful comments.

REFERENCES

- Abdelsalam H.M., Saha P. & Williams, L.L.R., 1998a, *New Astronomy Reviews*, 42, 157.
- Abdelsalam H.M., Saha P. & Williams, L.L.R., 1998b, *MNRAS*, 294, 734.
- Abdelsalam H.M., Saha P. & Williams, L.L.R., 1998c, *AJ*, 116, 1541.
- Bradac M., Schneider P., Lombardi M., Erben T., 2005, *A&A*, 437, 39.
- Bridle S.L., Hobson M.P., Lasenby A.N., Saunders R., 1998, *MNRAS*, 299, 895.
- Broadhurst T.J., Taylor A.N., Peacock J.A., 1995, *ApJ*, 438, 49.
- Broadhurst T., Benitez N., Coe D., Sharon K., Zekser K., White R., Ford H., Bouwens R., 2005a, *ApJ*, 619, 143.
- Diego J.M., Protopapas P., Sandvik H.B, Tegmark M. 2005a, *MNRAS*, 360, 477. (**Paper I**)
- Diego J.M., Sandvik H.B., Protopapas P., Tegmark M., Benitez N., Broadhurst T., 2005b, *MNRAS* in press. eprint arXiv:astro-ph/0412191 (**Paper II**)
- Gavazzi et al. 2004
- Hirata C.M. et al. **more than 8 authors**. 2005, *MNRAS*, 353, 529.
- Heymans C. et al. **more than 8 authors**. 2005, *MNRAS* submitted. preprint astro-ph/0506112.
- Kneib J.-P., Mellier Y., Fort B., Mathez G., 1993, *A&A*, 273, 367.
- Kneib J.-P., Mellier Y., Pello R., Miralda-Escudé J., Le Borgne J.-F., Boehringer H., & Picat J.-P. 1995, *A&A*, 303, 27.
- Kneib J.-P., Ellis R.S., Smail I.R., Couch W., & Sharples R. 1996, *ApJ*, 471, 643.
- Kneib J.-P., Hudelot P., Ellis R.S., Treu T, Smith G.P., Marshall P., Czoske O., Smail I.R., Natarajan P., 2003, *ApJ*, 598, 804.
- Kochanek, C.S., Schneider, P., Wambsganss, J., 2004, Part 2 of *Gravitational Lensing: Strong, Weak & Micro*, Proceedings of the 33rd Saas-Fee Advanced Course, G. Meylan, P. Jetzer & P. North, eds. (Springer-Verlag: Berlin. Preprint astro-ph/0407232.
- Press W.H., Teukolsky S.A., Vetterling W.T., Flannery B.P., 1997, *Numerical Recipes in Fortran 77*. Cambridge University Press.
- Saha, P., Williams, L.L.R., 1997, *MNRAS*, 292, 148.
- Saha, P., Williams, L.L.R., AbdelSalam H.M., 1999, astro-ph/9909249.
- Saha P. 2000, *AJ*, 120, 1654.
- Saha, P., Williams, L.L.R., 2004, *ApJ*, 127, 2604.
- Sand D.J., Treu T. Ellis R.S. 2002, *ApJ*, 574, 129.
- Sha F., Saul L.K., Lee D.D., 2002, *Advances in Neural Information Processing systems*, 15, 1065.
- Smith G.P., Kneib J.-P., Smail. I., et al. 2004, astro-ph/0403588.
- Treu T., Koopmans L.V.E., 2004, *ApJ*, 611, 739.
- Trotter C.S., Winn J.N., Hewitt J. N., 2000, *ApJ*, 535, 671.
- Warren S.J., Dye S., 2003, *ApJ*, 590, 673.
- Williams L.L.R., & Saha P., 2001, *AJ*, 119, 439.

This paper has been typeset from a \TeX / \LaTeX file prepared by the author.